Carrier Dynamics in Blue, Cyan, and Green InGaN/GaN LEDs Measured by Small-Signal Electroluminescence

Xuefeng Li[1*], Nick Pant[2,3], Elizabeth DeJong[1], Abdelrahman Tarief Elshafiey[1], Rob Armitage[4], Emmanouil Kioupakis[2], and Daniel Feezell[1]

[1]*Center for High Technology Materials (CHTM), University of New Mexico, Albuquerque, NM 87106, USA*
[2]*Department of Materials Science & Engineering, University of Michigan, Ann Arbor, MI 48109, USA*
[3]*Applied Physics Program, University of Michigan, Ann Arbor, MI 48109, USA*
[4]*Lumileds LLC, San Jose, CA 95131, USA*

We study the carrier dynamics for *c*-plane InGaN/GaN LEDs with various emission wavelengths near the green gap using a small-signal electroluminescence method. The LEDs were grown by Lumileds using state-of-the-art growth conditions. Radiative and non-radiative recombination rates are numerically separated, and the carrier recombination lifetime and carrier density are obtained. Experiment shows the causes of efficiency reduction at longer wavelength in the present structures are injection efficiency decrease, radiative recombination rate decrease, and imbalance of the increase of Auger-Meitner and radiative terms due to the interplay between the carrier-current density relationship and the quantum-confined Stark effect (QCSE). The effects of QCSE, phase-space filling, and the carrier-current density relationship on efficiency reduction at longer wavelengths are examined separately with experimental data and Schrödinger-Poisson calculations. In addition, we confirm the scaling law between $C(n)$ and $B(n)$ under electrical injection and find that the increase in carrier density at a given current density is the primary cause for lower radiative efficiency at high current density in longer wavelength LEDs. Conversely, we do not observe a significant efficiency reduction at longer wavelengths from extrinsic material degradation.

[*]**Electronic mail:** xuefengli@unm.edu

Blue and green InGaN/GaN light-emitting diodes (LEDs) are crucial for solid-state lighting and display applications [1,2]. Violet–blue LEDs have achieved a high EQE of ~80% [3,4]. However, InGaN/GaN LEDs still suffer from strong efficiency loss in the green region [5], which is usually referred to as the "green gap." The green gap issue has been related to Auger-Meitner recombination (the renaming proposal can be found in Ref. 6) [7-10], the quantum-confined Stark effect (QCSE) [11-14], carrier leakage [15,16], and defects and carrier localization [5,17-22], among other causes. To achieve longer emission wavelengths, the indium composition must be increased, leading to several problems. First, high indium content increases lattice mismatch [23] and can potentially introduce additional point defects [24] during metalorganic chemical vapor deposition (MOCVD). High indium content also leads to strong polarization-related electric fields in the quantum wells (QWs), lowering the wavefunction overlap and decreasing the radiative and non-radiative recombination rates (i.e., from the QCSE). Studying the carrier dynamics to understand the relative roles of intrinsic effects (e.g., wavefunction overlap, carrier-current density relationship, phase-space filling (PSF)) vs. extrinsic effects (e.g., material degradation due to increased defect density, compositional inhomogeneities, etc.) is critical to combating efficiency reduction in long-wavelength LEDs.

In this work, we use small-signal electroluminescence (SSEL) to study the carrier dynamics in *c*-plane LEDs with various emission wavelengths ranging from blue (~470 nm), to cyan (~500 nm), to green (~530 nm). The LED series consists of three wafers grown by Lumileds using state-of-the-art growth conditions with identical active region designs (3X, 3-nm-thick QWs) but indium compositions ranging from 16% to 19%, as measured by energy-dispersive X-ray spectroscopy (EDX). The barriers are GaN and are 18 nm thick. LEDs with mesa diameters of 100 μm and ground-signal-ground electrodes were fabricated. SSEL [25,26] was then used to study the carrier dynamics of the LEDs. Values for each element in an equivalent circuit model were acquired via simultaneous fitting of the impedance and modulation responses, leading to the injection efficiency and total carrier recombination lifetime. Combining the total carrier lifetime with the internal quantum efficiency (IQE) enables the separation of the radiative and non-radiative recombination lifetimes and rates as a function of current density (J) and carrier density (n). A common approach to describe the carrier recombination mechanisms uses the $A(n), B(n), C(n)$ parameters, which are associated with Shockley-Read-Hall (SRH), radiative, and Auger-Meitner recombination, respectively. The experiments reveal that efficiency loss at longer wavelength in the present structures is related to reduction in injection efficiency and confirm that a reduction in radiative recombination and an increase in Auger-Meitner recombination also reduce efficiency, as previously observed in Ref. 27 using optical differential lifetime (ODL) measurements. The

interplay between the QCSE and carrier-current density relationship is shown to determine the relative importance of the radiative ($B(n)n^2$) and non-radiative recombination rates ($A(n)n$ and $C(n)n^3$) as the indium content is increased.

The LEDs were biased at various DC currents and modulated with a network analyzer (E5061B, Keysight), from 500 kHz to 2 GHz. The amplitude for the small AC signal was ~20 mV, as a low modulation amplitude is especially important for low current density operation. The LEDs were probed using an RF probe (ACP40-GSG-150, Cascade) and the modulated light was collected into a photodetector (DET025AFC, Thorlabs). A low-noise RF amplifier (PE15A1007, Pasternack) was used to amplify the signal, which was then coupled back to the network analyzer. [26] We measured the LEDs to a current density (J) lower limit of 3 A/cm^2, due to the low light output power at low J.

In SSEL, the differential rate equations are formulated and differential parameters (e.g., differential injection efficiency, differential recombination lifetime, etc.) are acquired. Integration is used to convert from differential injection efficiency to injection efficiency. We define the injection efficiency as the current that recombines in the QWs divided by the total current injected into the LED, and the detail can be found in Ref. 28. The injection efficiency decreases at longer wavelengths, as shown in Figure 1(a), but approaches unity injection at high J. The internal quantum efficiency (IQE) shown in Figure 1(b) was obtained from Lumileds using external quantum efficiency (EQE) measurements on LEDs with known extraction efficiency. There is significant reduction in IQE at longer wavelengths, a trend that is characteristic of the green gap. The IQE varies from 43.6% (blue) to 34.4% (cyan) to 25.7% (green) at 40 A/cm^2. The radiative efficiency (η_r) is obtained from the IQE (η_{IQE}) and the injection efficiency (η_{inj}) using $\eta_{IQE} = \eta_{inj} * \eta_r$, and is shown in Figure 1(c).

From the differential rate equations in the QW and cladding layer, the carrier density is calculated using [27]:

$$n_w = \frac{1}{q * S * d} \int_0^I \eta_{\Delta inj} \tau_{\Delta rec} dI \quad (1)$$

Here, q is elementary charge, S is mesa area, d is total QW thickness, $\tau_{\Delta rec}$ is differential recombination lifetime, and $\eta_{\Delta inj}$ is differential injection efficiency.

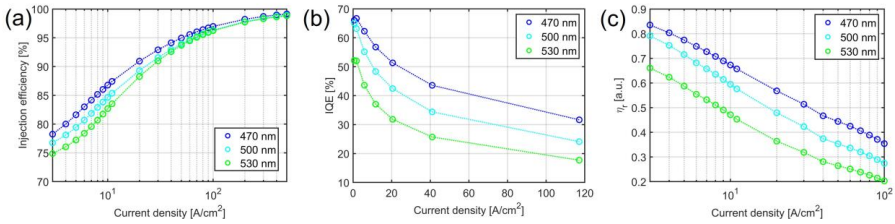

FIG. 1. (a) Injection efficiency, (b) IQE, and (c) Radiative efficiency for 470 nm, 500 nm, and 530 nm LEDs. Blue, cyan, and green colors represent 470 nm, 500 nm, and 530 nm wafers, respectively.

The carrier recombination lifetime (τ_{rec}) is obtained by integrating the differential recombination lifetime using the total recombination rate (R_{rec}) and the carrier density (n_w) [29, 30]:

$$R_{rec} = \int_0^{n_w} \frac{dn_w}{\tau_{\Delta rec}} \tag{2}$$

$$\tau_{rec} = \frac{n_w}{R_{rec}} \tag{3}$$

Moreover, quantitative analysis of the data collected using the SSEL method can separate the carrier recombination information into radiative and non-radiative components. The carrier recombination lifetime is given by $\frac{1}{\tau_{rec}} = \frac{1}{\tau_r} + \frac{1}{\tau_{nr}}$, and is composed of two parts: radiative recombination lifetime (τ_r) and non-radiative recombination lifetime (τ_{nr}). The radiative efficiency can then be written as: $\eta_r = \frac{\tau_{nr}}{\tau_{nr}+\tau_r}$. Then radiative and non-radiative recombination lifetimes can be acquired from: $\tau_r = \frac{\tau_{rec}}{\eta_r}$ and $\tau_{nr} = \frac{\tau_{rec}}{1-\eta_r}$. As shown in Figures 2(a) and 2(b), longer wavelength LEDs have longer radiative, non-radiative, and total recombination lifetimes. In Figure 2(b), the radiative lifetime is more sensitive to wavelength compared to the non-radiative lifetime, especially at high current densities. This results because $\frac{1}{\eta_r}$ is more sensitive to wavelength compared with $\frac{1}{1-\eta_r}$ at high current densities. The lower the value of η_r, the faster the change of $\frac{1}{\eta_r}$. Moreover, the nonradiative recombination lifetime increases at longer wavelengths, but the radiative lifetime increases even more, which leads to lower IQE at low *n* for longer wavelength.

The carrier-current density relationship depends on the strength of the internal electrical field in devices with different indium contents and directly relates to efficiency reduction. Since η_{inj} values are similar for all wavelengths at high *J*, the sum of the recombination rates is constant for different emission wavelengths at a given current density. At steady state, the carriers injected into the QW may recombine radiatively or non-radiatively:

$$\frac{J}{q * d} = A(n)n + B(n)n^2 + C(n)n^3 \tag{4}$$

At a given *J*, the $A(n), B(n)$, and $C(n)$ parameters for longer wavelengths are smaller due to the smaller wavefunction overlap and the corresponding carrier density increases to compensate for the larger QCSE. Figure 3(a) shows the carrier-current density relationship, confirming higher carrier density at a given current density for longer wavelength.

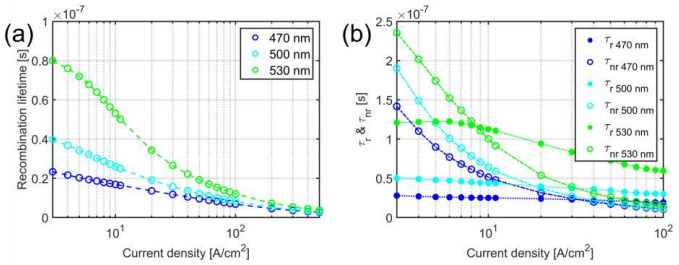

FIG. 2. (a) Total recombination lifetime and (b) Radiative and non-radiative lifetimes for 470 nm, 500 nm, and 530 nm LEDs.

The radiative and non-radiative recombination rates can be calculated from the carrier density in the active region and their respective lifetimes: $R_r = \frac{n_w}{\tau_r}$ and $R_{nr} = \frac{n_w}{\tau_{nr}}$. In Figure 3(b), the radiative recombination rate (R_r) is lower for longer wavelengths at a given current density, while the non-radiative recombination rate (R_{nr}) is higher for longer wavelengths. Since Auger-Meitner recombination is proportional to n^3, and biomolecular recombination is proportional to n^2, Auger-Meitner recombination will increase faster than radiative recombination at high *n*. In addition to increased Auger-Meitner recombination, reduction of the radiative rate is evidently an important cause of the green gap. In Figure 3(c), the radiative and non-radiative recombination rates are lower for longer wavelengths at a given carrier density. This is reasonable because the internal polarization field in the QW is stronger for long wavelength LEDs due to the high indium content, thus the wavefunction overlap is lower, and the $A(n), B(n)$, and $C(n)$ parameters are smaller. The reason for the different behaviors between R_r and R_{nr} vs. *J* and *n* lies in the interplay

between the carrier-current density relationship and QCSE. At longer wavelengths, the $A(n), B(n)$, and $C(n)$ parameters are lower, but the carrier density is higher at a given *J,* as shown in Figure 3(a).

To compute the $A(n)$, $B(n)$, and $C(n)$ coefficients, we use the standard approach of plotting G_{nr}/n, G_r/n^2, and $C(n) = (G_{nr} - A(n)n)/n^3$ [31]. As G_{nr}/n doesn't converge even at low n, the $C(n)$ parameter (Auger-Meitner recombination coefficient) is estimated based on the value of the $A(n)$ parameter. Two bounds are considered for $A(n)$: the lower bound is zero and the upper bound is $A(n) = G_{nr}/n$ at 3 A/cm^2. Details are available in the supplementary material. To further the understanding of the origin of the green gap, we calculate the ratios of $B(n)$, $C(n)$, and n for the green and cyan LEDs with respect to the blue LED with $A(n) = 0\ s^{-1}$, as shown in Figure 3(d). The ratio of $C(n)$ is not significantly affect by the value of $A(n)$, as the nonradiative recombination is dominated by Auger recombination at high *J*. Open circles, solid dots, and open squares denote the ratio of radiative recombination rates, non-radiative recombination rates, and carrier densities at a given *J*, respectively. The colors cyan and green represent the ratios between cyan/blue and green/blue, respectively. Normalized ratios for the various relevant parameters at 40 A/cm^2 are listed in Table 1. Here, we ignore the effect of SRH recombination and assume $C(n) \approx G_{nr}/n^3$, as Auger-Meitner recombination dominates at high *J*. It is clear that there is a similar relative decrease in $C(n)$ compared with $B(n)$ when the wavelength increases. For the cyan LED, $C(n)$ and $B(n)$ decrease to 55% and 48% compared to blue, respectively. For the green LED, $C(n)$ and $B(n)$ decrease to 15% and 14% compared to blue, respectively. Thus, the radiative and Auger-Meitner coefficients are affected by similar factors when the LED emission wavelength increases.

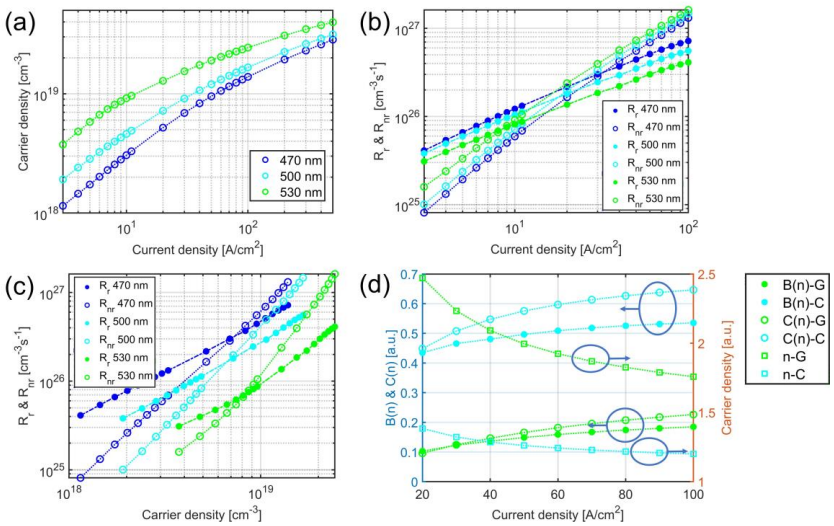

FIG. 3. Carrier dynamics for 470 nm, 500 nm, and 530 nm LEDs. (a) Carrier density vs current density. Radiative and non-radiative recombination rates vs. (b) current density and (c) carrier density. (d) Ratios of $B(n)$, $C(n)$, and n for cyan and green compared to blue.

Color	R_r	R_{nr}	n	$B(n)$	$C(n)$
Blue	1	1	1	1	1
Cyan	0.80	1.16	1.29	0.48	0.55
Green	0.60	1.34	2.09	0.14	0.15

Table 1. Normalized ratios of R_r, R_{nr}, n, $B(n)$, and $C(n)$ at 40 A/cm^2.

On the other hand, the carrier density in the green LED is more than 2X higher than the carrier density in the blue LED at 40 A/cm^2. Thus, the radiative efficiency reduction at longer wavelengths is more affected by the carrier-current density relationship than by extrinsic material degradation. At sufficiently high n where third-order intrinsic Auger-Meitner recombination dominates over SRH and second-order trap-assisted Auger-Meitner recombination [19, 32, 33], the radiative efficiency can be expressed as:

$$\eta_r = \frac{1}{1+\frac{R_{nr}}{R_r}} = \frac{1}{1+\frac{C(n)*n^3}{B(n)*n^2}} = \frac{1}{1+\frac{C(n)}{B(n)}*n} \quad (5)$$

In this limit, there are two factors that contribute to the radiative efficiency: the operating carrier density n and the ratio $C(n)/B(n)$. In Figure 4(a), we plot the experimental data for the relative $C(n)$ vs. $B(n)$ (see supplementary information) of the different LEDs. We observe universal linear scaling (i.e., $C(n) \propto B(n)^1$) for all three wavelengths over a range of carrier densities, which is consistent with the scaling law observed in III-nitride LEDs using an ODL technique [27]. Also included in Figure 4(a) is further verification of the linear scaling between $C(n)$ and $B(n)$ in these structures using 1D and 3D Schrödinger-Poisson calculations. This technique has been previously used to study recombination in InGaN quantum wells [11, 27, 34], and has most recently been successfully applied to model the optical spectrum of the green LEDs studied in the present work [35]. Figure 4(b) shows the ratios $C(n)/B(n)$ at different wavelengths for current densities higher than 8 A/cm^2. The ratio $C(n)/B(n)$ approaches $\sim 1.5 \times 10^{-19} cm^3$ with less than 25% deviation between different colors at high *n,* despite the fact that $B(n)$ and $C(n)$ individually vary by an order of magnitude from blue to green. This indicates that extrinsic material degradation does not play a major role in the green gap at high n for the LEDs studied. However, extrinsic material degradation was shown to have a significant impact on the efficiency of red InGaN/GaN LEDs with a higher indium composition [36]. To understand this, the recombination coefficients can be factorized into the product of an envelope wave-function overlap component (denoted hereafter with $|F|^2$) that includes the relative effects of polarization fields and phase-space filling and a bulk component that depends on the atomic wavefunctions. (For high n, the Coulomb enhancement term is close to unity due to free-carrier screening and can be ignored). Thus, $B(n) = |F_{eh}(n)|^2 B_{bulk}$, where $|F_{eh}(n)|^2$ corresponds to the thermally averaged overlap of the electron and hole wavefunctions. On the other hand, the C coefficient includes contributions from the eeh and hhe processes, where the excess energy of an electron-hole recombination is transferred to a nearby electron (eeh) or a nearby hole (hhe), $C(n) = |F_{eeh}(n)|^2 C_{eeh,bulk} + |F_{hhe}(n)|^2 C_{hhe,bulk}$. In polar III-nitride quantum wells, the intrinsic C coefficient is dominated by the hhe term, which in turn is proportional to the electron-hole overlap [33]. Thus, $C(n) \approx \kappa |F_{eh}(n)|^2 C_{hhe,bulk}$, where κ is a scaling constant that is the same across quantum wells of different wavelengths, according to theoretical calculations and experimental data of Figure 4(a). Putting these expressions together, the wavefunction overlaps, and thus the effects of polarization fields and phase-space filling, cancel out in the ratio $C(n)/B(n)$ (if n is large, as is the case here), leaving only the ratio of *bulk* recombination terms:

$$\frac{C(n)}{B(n)} \propto \frac{C_{hhe,bulk}}{B_{bulk}}. \quad (6)$$

According to DFT calculations of the intrinsic bulk recombination coefficients [37,38], $C_{hhe,bulk}/B_{bulk}$ is ~36% larger for green than for blue, and ~15% larger for cyan than for blue. For material degradation or extrinsic trap-assisted Auger-Meitner recombination to be responsible for the decline in the high-current radiative efficiency of InGaN LEDs with increasing wavelength, the ratio $C(n)/B(n)$ would have to substantially increase beyond ~36% from blue to green and ~15% from blue to cyan. In contrast, the experimental results of Figure 4(b) show that the $C(n)/B(n)$ ratios for LEDs of all three wavelengths are within a deviation of 25% from each other, a result that is consistent with the small variation in the ratio of intrinsic recombination coefficients calculated with DFT. This indicates that the behavior of $C(n)/B(n)$ for all three LEDs is consistent with theoretical expectations of the intrinsic recombination mechanics, and neither material degradation nor extrinsic trap-assisted Auger-Meitner recombination needs to be invoked.

Since *n* is more than 2X higher for the green LED compared to the blue LED at 40 A/cm^2, the radiative efficiency is mostly affected by larger *n,* resulting from lower $B(n)$ and $C(n)$ coefficients, rather than changes in $C(n)/B(n)$ at longer wavelengths. This is confirmed by plotting the radiative efficiency vs. *n* in Figure 4(c), which shows similar radiative efficiencies for all three wavelengths at a given *n*. However, LEDs operating at longer wavelengths should have less light output at a given *n*, as the *J* is lower for longer wavelengths at a given *n*. Thus, maintaining a low carrier density at a given *J* is critical to maintaining high efficiency at longer wavelengths. In InGaN/GaN LEDs, there are several possible paths to reduce the carrier density in the QWs by enhancing the wavefunction overlap and/or improving the inter-well carrier transport. Higher wavefunction overlap has been achieved with step potential profiles [39], nonpolar or semipolar orientations [40], or very thin QWs [41]. In addition, improving inter-well and lateral carrier transport using V-pit engineering is a very promising approach to achieve higher IQE in long-wavelength LEDs based on numerical modeling [42,43] and experiment [44-46].

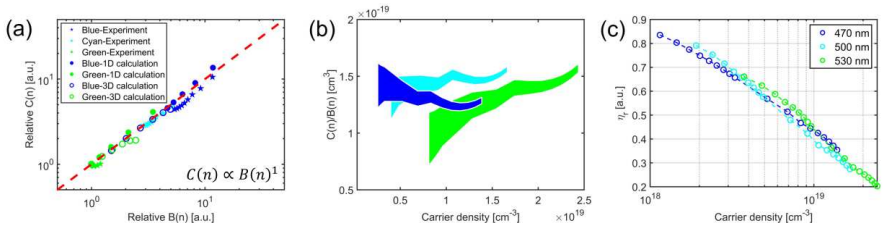

FIG. 4. Information at high n. (a) Relative $C(n)$ vs. $B(n)$ for experimental data, 1D, and 3D Schrödinger-Poisson calculations. Data from each method is normalized to green wavelength at highest n. (b) $C(n)/B(n)$ for the three wavelengths, (c) Radiative efficiency vs. n.

In summary, we studied the carrier dynamics of a series of LEDs with various emission wavelengths near the green gap using a small-signal electroluminescence method. Universal linear scaling between $C(n)$ & $B(n)$ was observed and $C(n)/B(n)$ approaches a similar value for all three wavelengths over a range of carrier densities, suggesting a small effect from extrinsic material degradation. However, the carrier density more than doubled in the green LED compared to the blue LED at 40 A/cm^2 due to the stronger QCSE in the green LED. The increase in carrier density at a given J for longer wavelengths had a much stronger effect than material degradation on reducing the radiative efficiency. Thus, approaches to increase the EQE of green LEDs should prioritize designs that decrease the carrier density in each QW, rather than focus on material quality improvement, particularly in LEDs that already have state-of-the-art epitaxy.

See the supplementary material for experimental data on $A(n)B(n)C(n)$ parameters and Schrödinger-Poisson calculations of $B(n)$ & $C(n)$.

This work was supported by the Department of Energy under Award No. DE-EE0009163. N. Pant acknowledges the support of the Natural Sciences & Engineering Research Council of Canada postgraduate scholarship.

[1] S. Pimputkar, J. S. Speck, S. P. DenBaars, and S. Nakamura, Nature Photon. 3, 180 (2009).
[2] S. Nakamura, M. Senoh, and T. Mukai, Japanese Journal of Applied Physics 32, (1993).
[3] Y. Narukawa, M. Ichikawa, D. Sanga, M. Sano, and T. Mukai, Journal of Physics D: Applied Physics 43, 354002 (2010).
[4] C.A. Hurni, A. David, M.J. Cich, R.I. Aldaz, B. Ellis, K. Huang, A. Tyagi, R.A. DeLille, M.D. Craven, F.M. Steranka, and M.R. Krames, Appl. Phys. Lett. 106, 031101 (2015).
[5] M. Auf der Maur, A. Pecchia, G. Penazzi, W. Rodrigues, and A. Di Carlo, Phys. Rev. Lett. 116, 027401 (2016).
[6] D. Matsakis, A. Coster, B. Laster, and R. Sime, Physics Today 72, 10 (2019).
[7] Y. C. Shen, G. O. Mueller, S. Watanabe, N. F. Gardner, A. Munkholm, and M. R. Krames, Appl. Phys. Lett. 91, 141101 (2007).

[8] J. Iveland, L. Martinelli, J. Peretti, J. S. Speck, and C. Weisbuch, Phys. Rev. Lett. 110, 177406 (2013).
[9] M. Binder, A. Nirschl, R. Zeisel, T. Hager, H.-J. Lugauer, M. Sabathil, D. Bougeard, J. Wagner, and B. Galler, Appl. Phys. Lett. 103, 071108 (2013).
[10] E. Kioupakis, P. Rinke, K.T. Delaney, and C.G. Van de Walle. Appl. Phys. Lett. 98, 161107 (2011).
[11] A. David and M.J. Grundmann, Appl. Phys. Lett. 97, 033501 (2010).
[12] E. Kioupakis, Q. Yan, and C.G. Van de Walle, Appl. Phys. Lett. 101, 231107 (2012).
[13] T. Takeuchi, S. Sota, M. Katsuragawa, M. Komori, H. Takeuchi, H. Amano, and I. Akasaki, Jpn. J. Appl. Phys., Part 2 36, L382 (1997).
[14] J. Bai, T. Wang, and S. Sakai, J. Appl. Phys. 88, 4729 (2000).
[15] M.-H. Kim, M. F. Schubert, Q. Dai, J. K. Kim, E. F. Schubert, J. Piprek, and Y. Park, Appl. Phys. Lett. 91, 183507 (2007).
[16] U. Ozgur, H. Liu, X. Li, X. Ni, and H. Morkoc, Proc. IEEE 98, 1180 (2010).
[17] B. Monemar and B. E. Sernelius, Appl. Phys. Lett. 91, 181103 (2007).
[18] J. Hader, J. V. Moloney, and S. W. Koch, Appl. Phys. Lett. 96, 221106 (2010).
[19] W. Liu, C. Haller, Y. Chen, T. Weatherley, J.-F. Carlin, G. Jacopin, R. Butté, and N. Grandjean, Appl. Phys. Lett. 116, 222106 (2020).
[20] S.Y. Karpov. Appl. Sci. 8(5), 818 (2018).
[21] D.S.P. Tanner, P. Dawson, M.J. Kappers, R. Oliver and S. Schulz. Phys. Rev. Applied 13, 044068 (2020).
[22] A. David, N.G. Young, C.A. Hurni, and M.D. Craven, Phys. Rev. Appl. 11, 031001 (2019).
[23] A. Lobanova, A. Kolesnikova, A. Romanov, S. Y. Karpov, M. Rudinsky, and E. Yakovlev, Appl. Phys. Lett. 103, 152106 (2013).
[24] S. Hammersley, M. J. Kappers, F. C.-P. Massabuau, S.-L. Sahonta, P. Dawson, R. A. Oliver, and C. J. Humphreys, Appl. Phys. Lett. 107, 132106 (2015).
[25] A. David, C.A. Hurni, N.G. Young, and M.D. Craven, Appl. Phys. Lett. 109, 033504 (2016).
[26] A. Rashidi, M. Nami, M. Monavarian, A. Aragon, K. DaVico, F. Ayoub, S. Mishkat-Ul-Masabih, A. Rishinaramangalam, and D. Feezell, J. Appl. Phys. 122, 035706 (2017).
[27] A. David, N.G. Young, C. Lund, and M.D. Craven, Appl. Phys. Lett. 115, 193502 (2019).
[28] A. Rashidi, M. Monavarian, A. Aragon, and D. Feezell, Appl. Phys. Lett. 113, 031101 (2018).
[29] L. A. Coldren, S. W. Corzine, and M. L. Mashanovitch, *Diode Lasers and Photonic Integrated Circuits* (John Wiley & Sons, 2012).
[30] A. Rashidi, M. Monavarian, A. Aragon, and D. Feezell, Sci. Rep. 9, 19921 (2019).
[31] A. David and M.J. Grundmann, Appl. Phys. Lett. 96, 103504 (2010).
[32] D.J. Myers, A.C. Espenlaub, K. Gelzinyte, E.C. Young, L. Martinelli, J. Peretti, C. Weisbuch, and J.S. Speck. Appl. Phys. Lett. 116, 091102 (2020).
[33] F. Zhou, M. Turiansky, A. Alkauskas, C.G. Van de Walle. arXiv:2211.08642 (2022).
[34] C.M. Jones, C.H. Teng, Q. Yan, P.C. Ku, and E. Kioupakis. Appl. Phys. Lett. 111, 113501 (2017).
[35] N. Pant, X. Li, E. DeJong, D. Feezell, R. Armitage, and E. Kioupakis. AIP Advances 12, 125020 (2022).
[36] H. Xue, S. Muyeed, E. Palmese, D.Rogers, R. Song, N. Tansu, and J. Wierer, IEEE Journal of Quantum Electronics, 59, 3200109 (2023).
[37] E. Kioupakis, D. Steiauf, P. Rinke, K.T. Delaney, and C.G. Van de Walle. Phys. Rev. B 92, 035207 (2015).
[38] E. Kioupakis, Q. Yan, D. Steiauf, and C.G. Van de Walle. New J. Phys. 15 125006 (2013).
[39] H. Zhao, G. Liu, J. Zhang, J.D. Poplawsky, V. Dierolf, and N. Tansu, Optics Express 19, (2011).
[40] M. Monavarian, A. Rashidi, and D. Feezell, Physica Status Solidi (a) 1800628, (2018).
[41] D.S.P. Tanner, J.M. McMahon, and S. Schilz, Phys. Rev. Applied 10, 034027 (2018).
[42] C.-K. Li, C.-K. Wu, C.-C. Hsu, L.-S. Lu, H. Li, T.-C. Lu, and Y.-R. Wu, AIP Advances 6, 055208 (2016).
[43] C.-H. Ho, J.S. Speck, C. Weisbuch, and Y.-R. Wu, Phys. Rev. Applied 17, 014033 (2022).
[44] R. Armitage, T. Ishikawa, H.J. Kim, and I. Wildeson, Light-Emitting Devices, Materials, and Applications XXVI (2022).
[45] S. Zhou, X. Liu, H. Yan, Y. Gao, H. Xu, J. Zhao, Z. Quan, C. Gui, and S. Liu, Sci. Rep. 8, 11053 (2018).
[46] F. Jiang, J. Zhang, L. Xu, J. Ding, G. Wang, X. Wu, X. Wang, C. Mo, Z. Quan, X. Guo, C. Zheng, S. Pan, and J. Liu, Photonics Research 7, 144 (2019).

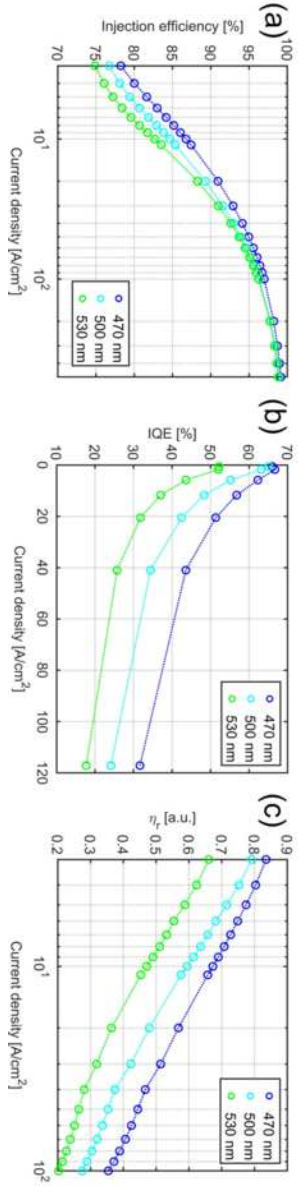

Applied Physics Letters

PLEASE CITE THIS ARTICLE AS DOI: 10.1063/5.0151301

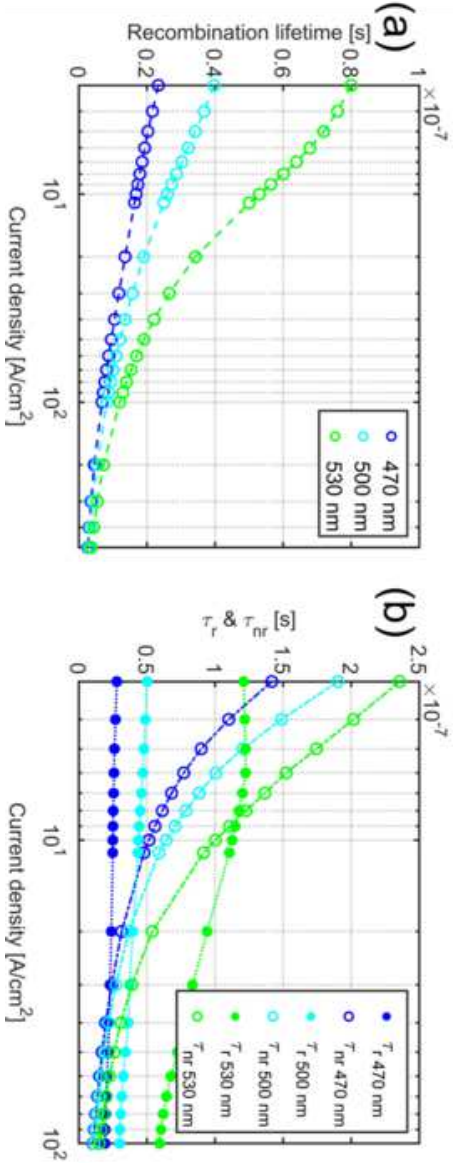

PLEASE CITE THIS ARTICLE AS DOI: 10.1063/5.0151301

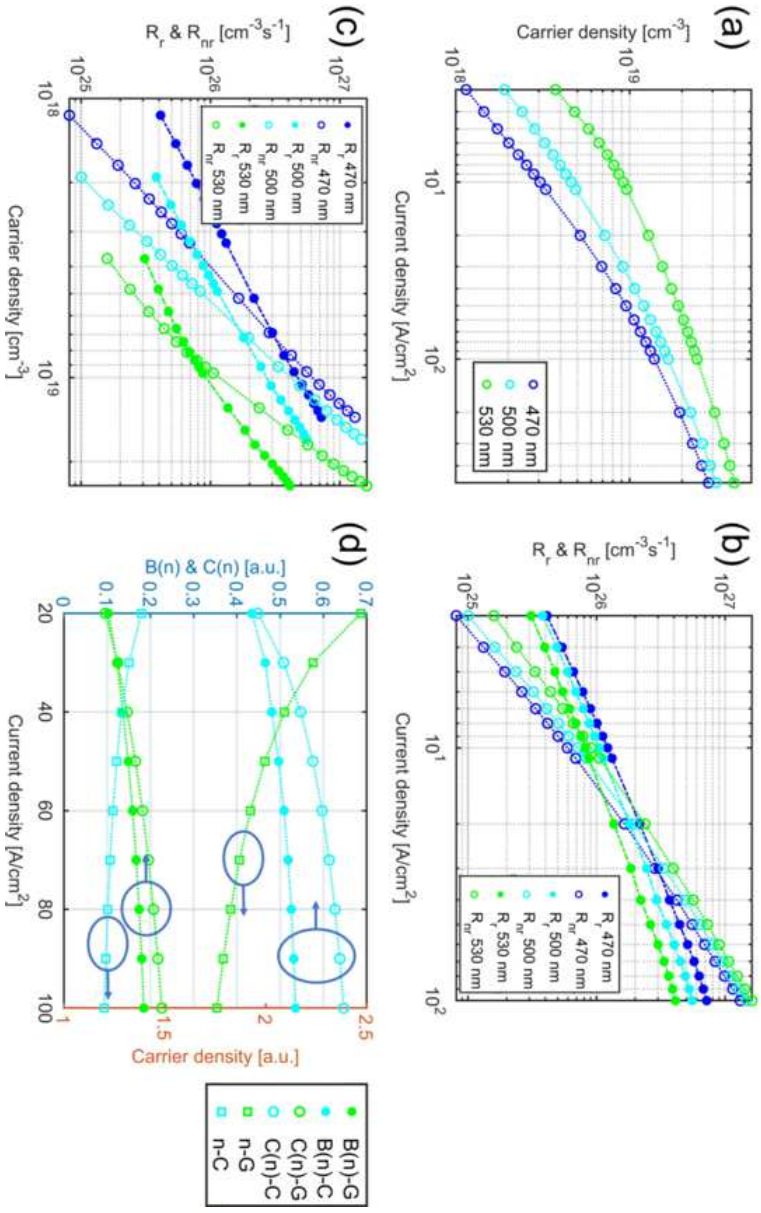

PLEASE CITE THIS ARTICLE AS DOI: 10.1063/5.0151301